

Hazard Assessment Comparison of Tazhiping Landslide Before and After Treatment using the Finite Volume Method

Dong Huang¹, YuanJun Jiang^{1*}, JianPing Qiao¹, Meng Wang¹

1. Key Laboratory of Mountain hazards and Surface process, Institute of Mountain hazards and Environment, Chinese Academy of Science, Chengdu 610041, China

*Corresponding author (yuanjun.jiang.civil@gmail.com).

Abstract: Through investigation and analysis of geological conditions and mechanical parameters of the Tazhiping landslide, Finite Volume Method coupling with Vollmy model is used to simulate the landslide mass movement process. The present paper adopts the numerical approach of RAMMS and the GIS platform to simulate the mass movement process before and after engineering treatment. This paper also provides the conditions and characteristic variables of flow-type landslide in terms of flow height, velocity, and stresses. The 3D division of hazard zones before and after engineering treatment was also mapped. The results indicate that the scope of hazard zones decreased after engineering treatment of the landslide. Compared with the case of before engineering treatment, the extent of high-hazard zones was reduced by about 2/3, and the characteristic variables of the mass movement in the case of after treatment decreased to 1/3 of those in the case of before treatment. Despite having engineering treatment, the Tazhiping landslide still poses significant potential threat to the nearby residences. Therefore, it suggests that the houses located in high-hazard zones should be relocated or reinforced for protection.

Keywords: finite volume method; rheological model; motion feature parameters; hazard assessment

1. Introduction

The hazards of a landslide include scope of influence (i.e., source area, possible path area, and backward and lateral expansion area) and secondary disasters (i.e., reservoir surge, blast, and landslide-induced barrier lake). A typical landslide hazard assessment aims to propose a systematic hazard assessment method with regard to a given position or a potential landslide. Current research on typical landslide hazard assessment remains immature, and there are multiple methods for interpreting landslide hazards. To be specific, the scope of influence prediction of a landslide refers to deformation and instability characteristics such as sliding distance, movement speed, and bulking thickness range. The movement behavior of a landslide mass is related to its occurrence, sliding mechanisms, mass characteristics, sliding path, and many other factors. Current landslide movement prediction methods include empirical prediction and numerical simulation.

Empirical prediction method: The empirical prediction method involves

44 analyzing landslide flow through the collection of landslide parameters in the field. It
45 further consists of the geomorphologic method (Costa, 1984; Jackson et al., 1987;
46 Scott et al., 1993), the geometric change method (Finlay et al., 1999; Michael-Leiba et
47 al., 2003), and the volume change method (Fannin et al., 2001). Empirical models are
48 commonly simple and easy to apply, and the required data are easy to obtain as well.
49 **Numerical simulation method:** Numerical simulation methods are further divided
50 into the continuous deformation analysis method (Hung, 1995; Evans et al., 2009;
51 Wang, et al., 2016), the discontinuous deformation analysis method (Shi, 1988), and
52 the simplified analytical simulation method (Christen et al., 2010a; Sassa, 2010;
53 Bartelt et al., 2012; Du et al., 2015). The numerical simulation method expresses
54 continuous physical variables using the original spatial and temporal coordinates with
55 geometric values of discrete points. Numerical simulations follow certain rules to
56 establish an algebraic equation set in order to obtain approximate solutions for
57 physical variables.

58 Empirical prediction models only provide a simple prediction of the sliding path.
59 Due to the differences in geological environments, empirical prediction models
60 commonly have low generality. Landslides move downslope in many different ways
61 (Varnes, 1978). In addition, landslides can evolve into rapidly travelling flows, which
62 exhibit characteristics of debris flows on unchannelized or only weakly channelized
63 hillslopes. The geomorphic heterogeneity of rapid shallow landslides, such as
64 hillslope debris flows, is larger than observed in channelized debris flows; however
65 many of these flows can be successfully modelled using the Voellmy-fluid friction
66 (Christen et al., 2012). The selection of model parameters remains one of the
67 fundamental challenges for numerical calculations of natural hazards.

68 The continuous deformation method has the advantage of an extremely strong
69 replication capability, but it is not recommended when analyzing flow-type landslides,
70 lahars, or debris flows because of complicated rheological behaviors (Iverson et al.,
71 1997, 2001; Hung et al., 2001; Glade 2005; Portilla et al., 2010; Chen et al., 2014).
72 The fluid mechanics-based discontinuous deformation method has several
73 shortcomings such as, great computational burden, difficult parameter selection, and
74 difficult 3D implementation. The simplified analytical simulation method fully takes
75 into account the flow state properties of landslides before introducing a rheological
76 model and can easily realize 3D implementation on the GIS platform. On that account,
77 this paper adopted the continuous fluid mechanics-based finite volume method
78 (simplified analytical simulation method). We introduce a rheological model on the
79 basis of using mass as well as momentum and energy conservation to describe the
80 movement of landslides. We also employed GIS analysis to simulate the entire
81 movement process of Taziping landslide and map the 2D division of hazard zones.

82

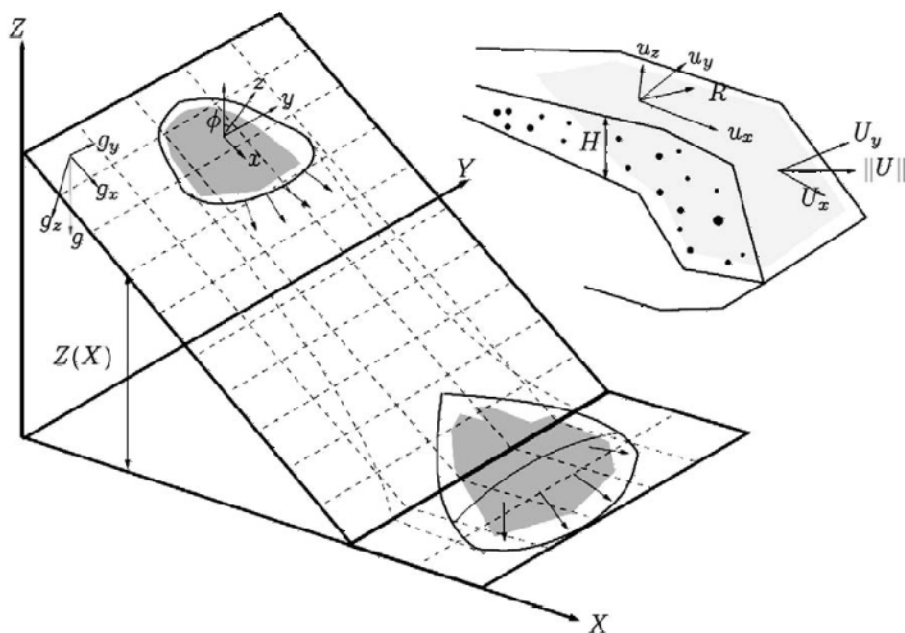
83 **2. Methods**

84 **2.1 Kinetic analysis method**

85 Adopting the continuous fluid mechanics-based finite volume method, this paper
86 took into account erosion action on the lower surface of the sliding mass and the

87 change in frictional resistance within the landslide-debris flow in order to establish a
 88 computational model. The basic idea is to divide the calculation area into a series of
 89 non-repetitive control volumes, ensuring that there is a control volume around each
 90 grid point. Each control volume is then integrated by the unresolved differential
 91 equation in order to obtain a set of discrete equations. The unknown variable is the
 92 numerical value of the dependent variable at each grid point. To solve the integral of a
 93 control volume, we make a hypothesis about the change rule of values among grid
 94 points, that is, about their piecewise distribution profile. The finite volume method
 95 can satisfactorily overcome the finite element method's weakness of slow calculation,
 96 and solve the problem of complex region processing. Thus, we adopted the finite
 97 volume method to establish the kinematic model for the landslide flow process.

98 The core of the finite volume method is domain discretization. The finite volume
 99 method uses discrete points as a substitute for continuous space. The physical
 100 meaning of the discrete equation is the conservation of the dependent variable in a
 101 finite control volume. Establishment of the conservation equation is based on the
 102 continuous movement model, that is, the continuity hypothesis about landslide
 103 substances. We divided the landslide mass into a series of units and made the
 104 hypothesis that each unit has consistent kinematic parameters (speed at a depth,
 105 density, etc.) and physical parameters (Fig.1). We also established an Eulerian
 106 coordinate system-based conservation equation with regard to each control volume.



107
 108 Fig.1 Schematic diagram of finite volume discretization (Christen et al., 2010a).
 109

109 2.2 Control equation

110 The computational domain is defined as directions x and y , and the
 111 topographic elevation is given the coordinate $z(x, y)$. $H(x, y, t)$ is assumed as the
 112 change relationship of landslide thickness with time; $U_x(x, y, t)$ and $U_y(x, y, t)$

113 respectively represent the mean movement speeds along directions x and y at
 114 moment t ; $n_x = U_x / \sqrt{U_x^2 + U_y^2}$ and $n_y = U_y / \sqrt{U_x^2 + U_y^2}$ represent the cosinoidal and
 115 sinusoidal flow vectors of the landslide on the plane $x - y$. The mean flow speed of
 116 substances is defined as $U = \sqrt{U_x^2 + U_y^2}$.

117 Thus, the mass balance equation becomes:

$$118 \quad \partial_t H + \partial_x (HU_x) + \partial_y (HU_y) = \dot{Q} \quad (1)$$

119 wherein, $\dot{Q}(x, y, t)$ represents the change rate (entrainment rate) of landslide
 120 volume with time.

121 Assuming that $l(x, y, t)$ represents the movement distance of the landslide with
 122 time, we can obtain:

$$123 \quad \dot{Q} = \begin{cases} 0 & \text{if } h_i = 0 \\ \frac{\rho_i}{\rho_a} h_i \frac{U}{l} & \text{if } k_i l \geq h_i \\ \frac{\rho_i}{\rho_a} k_i U & \text{if } k_i l < h_i \end{cases} \quad (2)$$

124 wherein, h_i represents the thickness of the i th layer of the landslide in the
 125 movement process; ρ_i represents the density of the i th layer of the landslide in the
 126 movement process; ρ_a represents the density of the landslide; the dimensionless
 127 parameter k_i represents the entrainment rate.

128 The momentum balance equation is:

$$129 \quad \partial_t (HU_x) + \partial_x (HU_x^2 + \frac{g_z k_{a/p} H^2}{2}) + \partial_y (HU_x U_y) = S_{gx} - S_f(R)[n_x] \quad (3)$$

$$130 \quad \partial_t (HU_y) + \partial_y (HU_y^2 + \frac{g_z k_{a/p} H^2}{2}) + \partial_x (HU_x U_y) = S_{gy} - S_f(R)[n_y] \quad (4)$$

131 wherein, $S_{gx} = g_x H$ and $S_{gy} = g_y H$ represent the dynamic components of the
 132 acceleration of gravity in directions x and y ; $g = (g_x \ g_y \ g_z)$ represents the
 133 vector of the acceleration of gravity; $k_{a/p}$ represents the pressure coefficient of soil;

134 ρ_a represents the density of the landslide; the dimensionless parameter k_i
 135 represents the entrainment rate; $S_f(R)$ represents the frictional resistance.

136 The kinetic energy balance equation is:

$$137 \quad \partial_t(HR) + \partial_x(HRU_x) + \partial_y(HRU_y) = \dot{P} - \dot{D} \quad (5)$$

138 wherein, $R(x, y, t)$ represents the random mean kinetic energy of the landslide;
 139 $\dot{P}(x, y, t)$ and $\dot{D}(x, y, t)$ represent the random increased kinetic energy and decreased
 140 kinetic energy of the landslide.

141 2.3 Constitutive relationship

142 The improved Voellmy rheological model is applied in the computational
 143 simulation of the landslide. See the computational formula below:

$$144 \quad S_f = \frac{u_i}{\|U\|} (h\mu g_z + R_i U^2 + R_\zeta U^2) \quad (6)$$

$$145 \quad R_i = \mu h \frac{U^T K U}{U^2}, R_\zeta = \frac{g}{\zeta} \quad (7)$$

146 wherein, $u_i/\|U\|$ represents the unit vector in the movement direction of the
 147 landslide; μ represents the Coulomb friction coefficient, and is related to $R(x, y, t)$,
 148 the random mean kinetic energy of the landslide; R_i represents the gravity-related
 149 frictional force coefficient; K represents the substrate surface curvature; ζ
 150 represents the viscous friction coefficient of the ‘‘turbulent flow’’.

151 2.4 HLLE-Heun numerical solution

152 Synthesizing control equations (1), (3), (4) and (5), we can obtain the simplified
 153 form of the nonlinear hyperbola equation:

$$154 \quad \partial_t V + \nabla \cdot F(V) = G(V) \quad (8)$$

$$155 \quad V = \begin{pmatrix} H \\ HU_x \\ HU_y \\ HR \end{pmatrix} \quad G(V) := \begin{pmatrix} \dot{Q} \\ S_{gx} - S_{fx} \\ S_{gy} - S_{fy} \\ \dot{P} - \dot{D} \end{pmatrix}$$

$$F(V) = \begin{pmatrix} HU_x & HU_y \\ HU_x^2 + g_z k_{a/p} \frac{H^2}{2} & HU_x U_y \\ HU_x U_y & HU_y^2 + g_z k_{a/p} \frac{H^2}{2} \\ HRU_x & HRU_y \end{pmatrix}$$

157 wherein, $V(x, y, t)$ represents a vector equation consisting of four unknown
 158 vector variables; $F(V)$ represents the flux function; $G(V)$ represents the source
 159 term. Based on the HLLE equation of the finite volume method and the quadrilateral
 160 grid, the node layout can adopt the grid center pattern, and the normal flux along one
 161 side of the control volume can be represented by the flux at the center of the side. The
 162 finite volume discretization adopting the control volume as unit is depicted in Fig.1;
 163 the Gauss theorem can be followed for the integration of equation (8), wherein C_i
 164 represents the unit volume; after converting the volume integral flux function $F(V)$
 165 into the curved surface integral, we can obtain:

$$\int_{C_i} \partial_t V dx + \iint_{\partial C_i} F(V) \cdot n_i d\sigma = \int_{C_i} G(V) dx \quad (9)$$

167 wherein, n_i represents the outward normal direction vertical to unit C_i at the
 168 boundary; through adopting the HLL format for the discretization of surface integral,
 169 the following simplified form can be obtained:

$$V_i^{(*)} = V_i^{(n)} + \frac{\Delta t}{A_{C_i}} \Delta F_i^{(HLL)}(V^{(n)}) \quad (10)$$

$$V_i^{(**)} = V_i^{(*)} + \frac{\Delta t}{A_{C_i}} \Delta F_i^{(HLL)}(V^{(*)}) \quad (11)$$

$$V_i^{(n+1)} = \frac{1}{2} (V_i^{(n)} + V_i^{(**)}) \quad (12)$$

173 wherein, $V_i^{(n)}$ represents the mean value of unit variables at moment $t^{(n)}$; $V^{(n)}$
 174 represents the mean value of the entire grid at moment $t^{(n)}$; $\Delta t := t^{(n-1)} - t^{(n)}$ represents
 175 the calculated time step; A_{C_i} represents the area of unit C_i ; $\Delta F_i^{(HLL)}$ represents the
 176 approximate value of the curved surface integral, as shown below:

$$\Delta F_i^{(HLL)}(V^{(n)}) := - \sum_{j=1}^4 F_{ij}^{(HLL)}(V^{(n)}) n_{ij} \Delta X \quad (13)$$

178 wherein, n_{ij} represents the outward normal direction of the i th unit at

179 boundary j ; the flux calculation term $F_{ij}^{(HLL)}(V^{(n)})$ represents the approximate
 180 solution mode of the Riemann problem of the i th unit at boundary j ; see the
 181 computational formula below:

$$182 \quad F_{ij}^{(HLL)}(V^{(n)}) = \begin{cases} F(V_L^{(n)}) & 0 \leq S_L \\ \frac{S_R F(V_L^{(n)}) - S_L F(V_R^{(n)}) + S_R S_L F(V_R^{(n)} - V_L^{(n)})}{S_R - S_L} & S_L \leq 0 \leq S_R \\ F(V_R^{(n)}) & S_R \leq 0 \end{cases} \quad (14)$$

183 wherein, $V_L^{(n)}$ and $V_R^{(n)}$ respectively represent the approximate values of $V^{(n)}$
 184 on both sides of boundary j of the i th unit; S_L and S_R respectively represent the
 185 wave speeds on the left and right sides. Refer to the computational method described
 186 by Toro (1992). In addition, the gradient magnitude in the original second-order
 187 difference equation can be limited through multiplication with the flux limiter, and the
 188 second-order format of the TVD property can be constructed to avoid the occurrence
 189 of numerical oscillation. Refer to the specific method described by LeVeque (2002).

190 In this paper a numerical solver within RAMMS is used, which was specifically
 191 designed to provide landslide (avalanche) engineers with a tool that can analyze
 192 problems with two-dimensional depth-averaged mass and momentum equations on
 193 three-dimensional terrain using both first and second-order finite volume methods
 194 (Christen et al., 2010b). Therefore, the finite volume method is adopted to analyze the
 195 the flow-type (high mobility, high velocity, large scope of risks, etc.) of the landslide
 196 mass movement process. The present paper adopts the numerical approach of
 197 RAMMS and the GIS platform to simulate the mass movement process before and
 198 after treatment. The landslide depositional characteristics and the mass movement
 199 conditions can be combined to provide a scientific basis for engineering prevention ,
 200 control, and forecast risk assessments for these kinds of disasters.

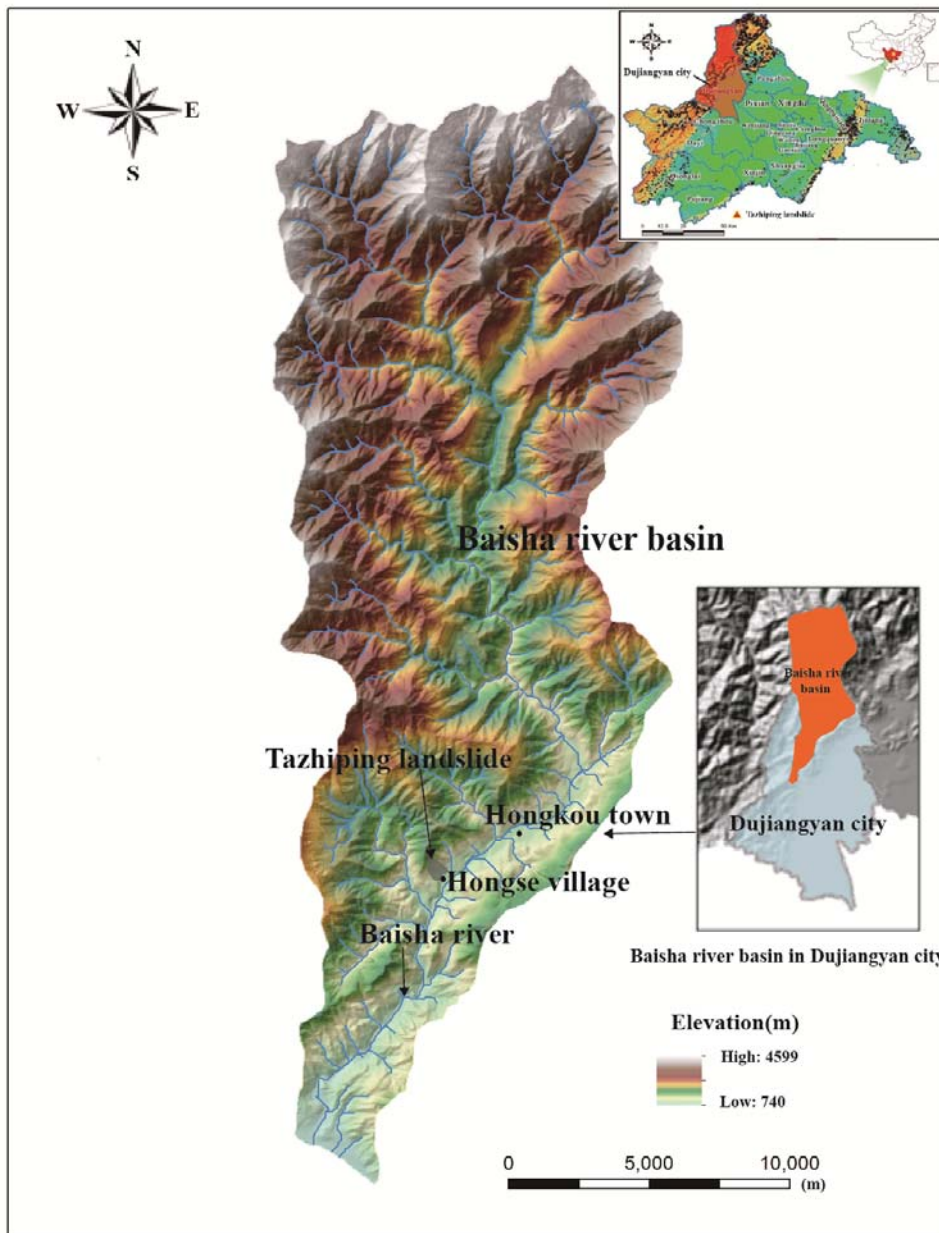
201

202 **3. Study area and data**

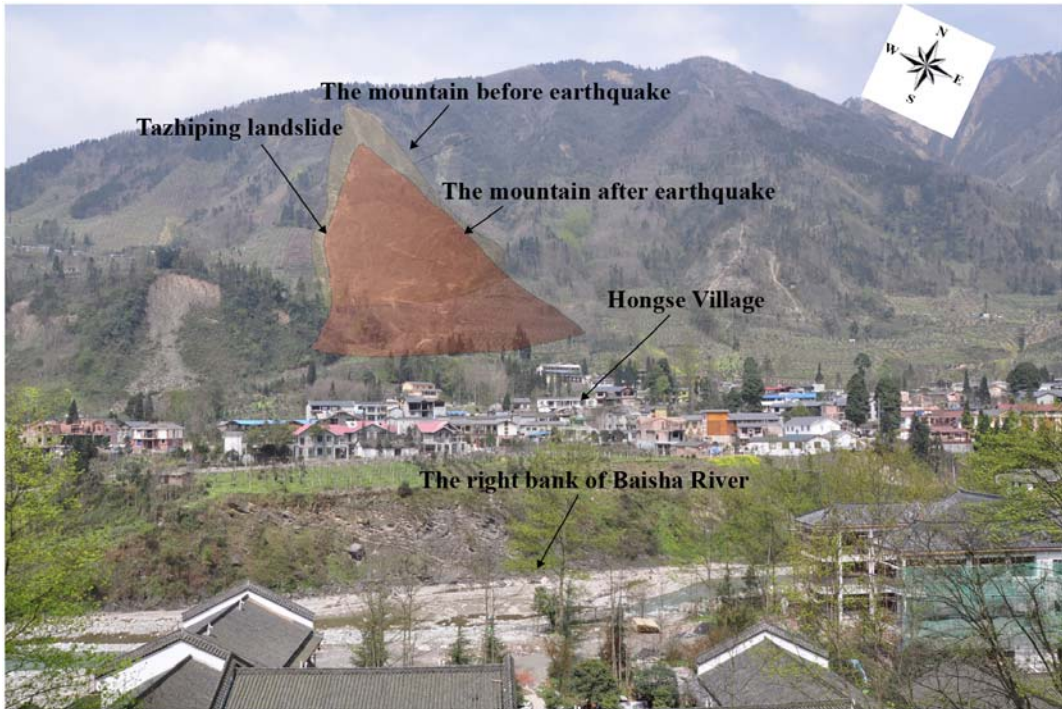
203 **3.1 Taziping landslide**

204 The Taziping landslide is located southeast of the Hongse Village, Hongkou
 205 Town, Dujiangyan City of Sichuan Province. The site is located at (E103°37'46",
 206 N31°6'29"), 68 km west Chengdu City and 20 km from the Dujiangyan Urban
 207 District (Fig. 2). Its geomorphic unit is a middle-mountain tectonic erosional area on
 208 the north bank of the Baisha River Valley. The Taziping Landslide is a large-scale
 209 colluvial layer landslide triggered by the Wenchuan Earthquake (Fig. 3). It has a
 210 gradient of 25°-40° with an average gradient of 32°. The landslide has an apparent
 211 round-backed armchair contour with a steep rear edge, which has a gradient of
 212 35°-50° and an elevation of about 1,370 m. The front edge is located on the south side
 213 of the mountain road, and has an elevation of about 1,007 m. The landslide has an

214 elevation difference of about 363 m, and a main sliding direction of 124°NE. The
 215 landslide mass forms an irregular semi-elliptical shape, and has a length of about 530
 216 m, an average width of 145 m and an area of approximately $7.68 \times 10^4 \text{ m}^2$. The
 217 landslide mass is composed of gravelly soil and is covered on by silty clay mingled
 218 with gravel. In terms of spatial distribution, the landslide is thick in the middle and
 219 thin on the lateral edges, has a thickness of 20-25 m and a volume of approximately
 220 $1.16 \times 10^6 \text{ m}^3$. During the earthquake, the landslide mass slid to cover the northern
 221 mountain slope of the Hongse Village Miaoba settlement. The landslide has an
 222 apparent front edge boundary, and there is also a swelling deformation (Fig. 4).



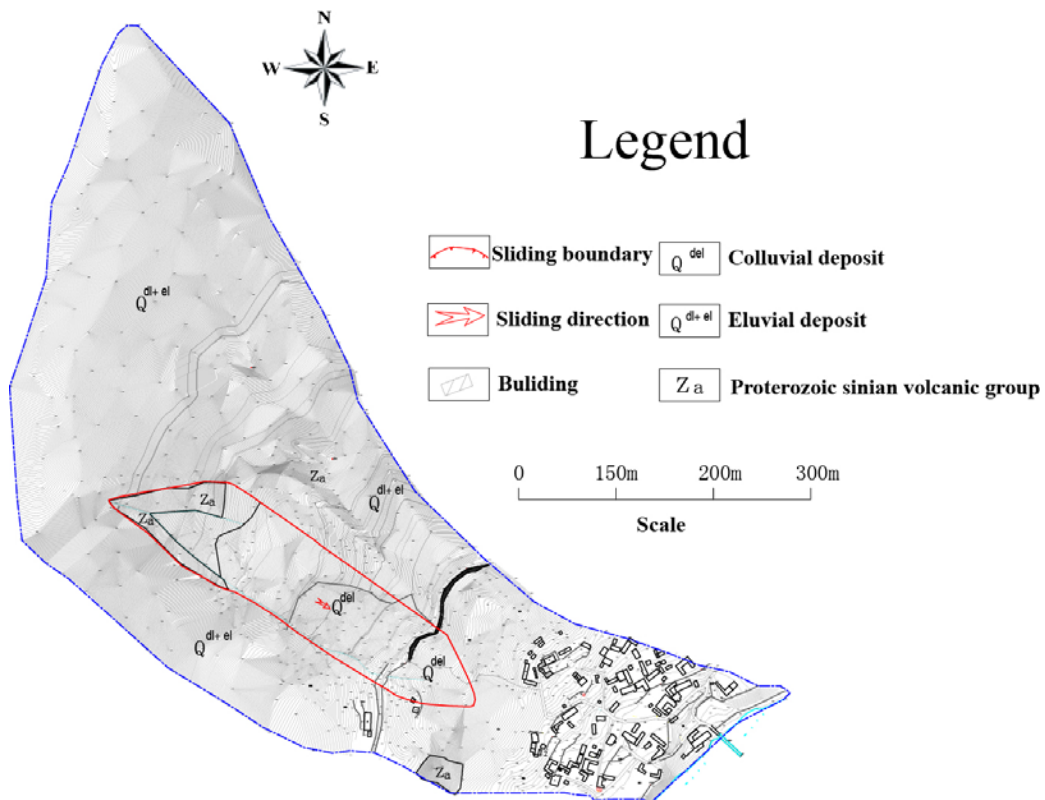
223
 224 Fig.2 Location of Tazhiping landslide, Baisha river basin, Dujiangyan city (the
 225 landslide was triggered by Wenchuan Ms 8.0 earthquake on May 12, 2008)



226

227

Fig.3 Tazhiping Landslide



228

229

Fig.4 Plane sketch of the Tazhiping landslide

230

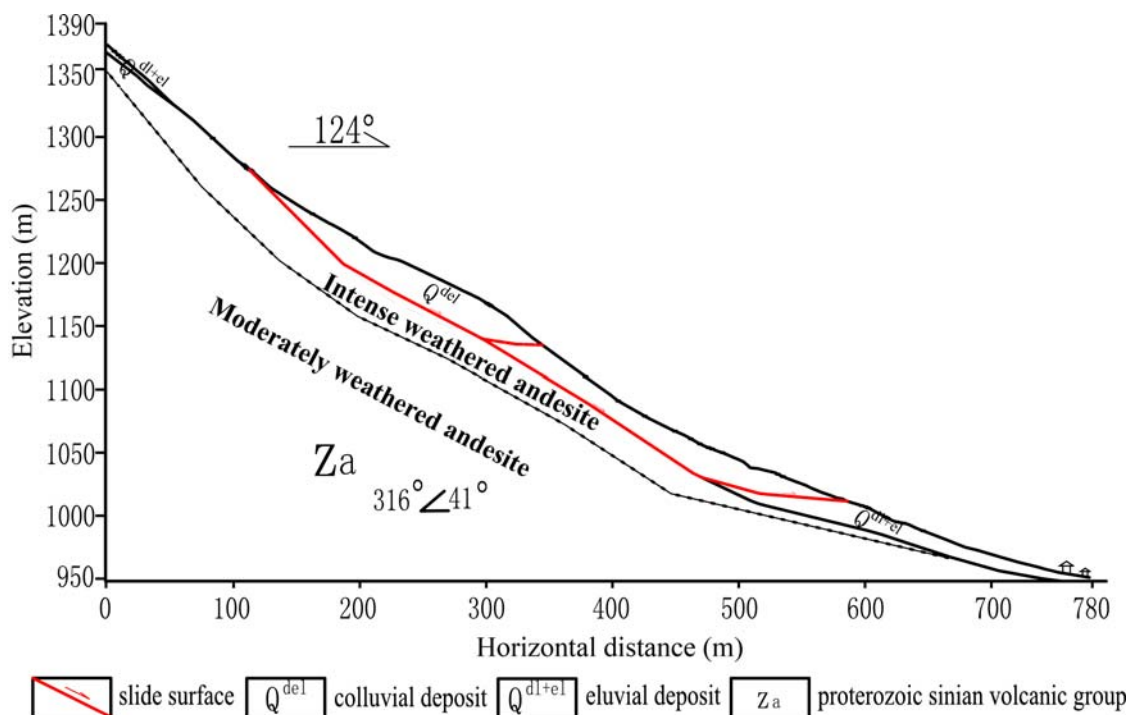
After the Wenchuan Earthquake, the massive colluvial deposits covered the mountain slope. The colluvium is 0.5-5.0 m thick at the top of the slide and is composed of rubble and gravel. The mass consists of a small amount of fine gravel,

232

233 which is composed of gray or grayish-green andesite with a clast of 20-150 cm. Field
 234 surveys indicate that the rubble in the surface layer has a maximum diameter
 235 exceeding 2 m, and that fine gravel is loosely intercalated with the rubble. A small
 236 amount of yellowish-brown and gray-brown silty clay mixed with 5-40% of
 237 non-uniformly distributed rubble composed the first 5-10 m of the slide. From 10-25
 238 m deep, there is a wide distribution of gravelly soil. The soil is grayish-green or
 239 variegated in color, is slightly compact and non-uniform, and has a rock fragment
 240 content of about 50%. The parent rock of the rock fragments is andesite, filled with
 241 silty clay or silt (Fig.5). Table 1 shows the parameters of the surface gravelly soil of
 242 the landslide mass based on the field sampling.

243 Tab.1 Parameters of surface soil of Taziping Landslide

Internal friction angle (°)		Cohesion (kPa)	Relative compactness	Natural void ratio	Dry density (kN·m ⁻³)	Specific gravity (g·cm ⁻³)
Peak	Residual					
27.5	23	20.5	53%	0.789	15.357	2.492



244

245 Fig.5 Geological profile of the Taziping Landslide

246 The landslide is an unconsolidated mass containing relatively large amounts of
 247 crushed stones and silty clay (Fig.6). Its loose structure and strong permeability
 248 facilitate infiltration of surface water. The Wenchuan earthquake aggravated the
 249 deformation of the landslide making deposits more unconsolidated, further reducing
 250 the stability of the landslide mass. During persistent rainfall, surface water infiltrates
 251 the landslide slope resulting in increased water pressure within the landslide mass and

252 reduced shear strength on the sliding surface. Thus, rainfall constitutes the primary
 253 inducing factor of the upper Taziping landslide. After infiltrating the loose layer, water
 254 saturates the slope increasing the dead weight of the sliding mass and reducing the
 255 shear strength of soil in the sliding zone. Infiltration into the landslide mass also
 256 increases the infiltration pressure of perched water, drives deformation, and poses a
 257 great threat to villages located at the front of the landslide. Slide-resistant piles and
 258 backfill were place at the toe of the slope in order to reduce the hazards of future
 259 slides. The slide-resistant piles have enhanced the overall stability of the slope,
 260 however, under heavy rainfall the upper unconsolidated landslide deposits may cut
 261 out from the top of the slide-resistant piles.



262

(a) Material on the landslide surface (b) Material in the shear zone

263

Fig.6 Photographs showing colluvial deposit cover on the mountain slope

264

265 Therefore we simulate possible movement states of the Taziping landslide before
 266 and after treatment with slide-resistant piles, comparatively analyzed the kinetic
 267 parameters in the movement process, and mapped the 2D division of hazard zones.

268

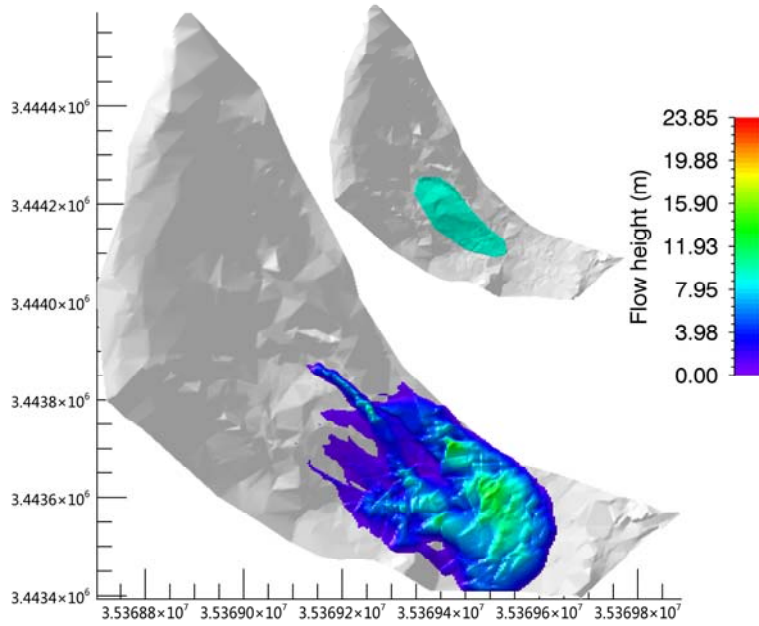
3.2 Hazard prediction before treatment

269

270 It was assumed that the landslide was damaged before engineering treatment.
 271 According to field investigation, the sliding mass had an estimated starting volume of
 272 about $600,000\text{m}^3$ and a mean thickness of 8m. Based on the survey report and field
 273 investigation (Hydrologic Engineering and Geological Survey Institute of Hebei
 274 Province, 2010), we adopted the survey parameters of Tab.2 for the simulated
 275 calculation. These parameters were obtained from laboratory or small-scale
 276 experiments and back-analyses of relatively well-documented landslide cases. The
 277 unit weigh $\gamma = 20.8\text{kN} \cdot \text{m}^{-3}$ is from small-scale conventional
 278 triaxial test experiments in laboratory. In addition, we selected the coulomb friction
 279 coefficient $\mu = 0.45$ and viscous friction coefficient $\zeta = 500\text{m} \cdot \text{s}^{-2}$ in accordance
 280 with back-analyses of well-documented landslide cases (Cepeda et al., 2010; Du et al.,
 281 2015). The erosional entrainment rate selected was the minimum value $k_i = 0.0001$
 282 in the RAMMS program.

Tab.2 Model calculation parameters

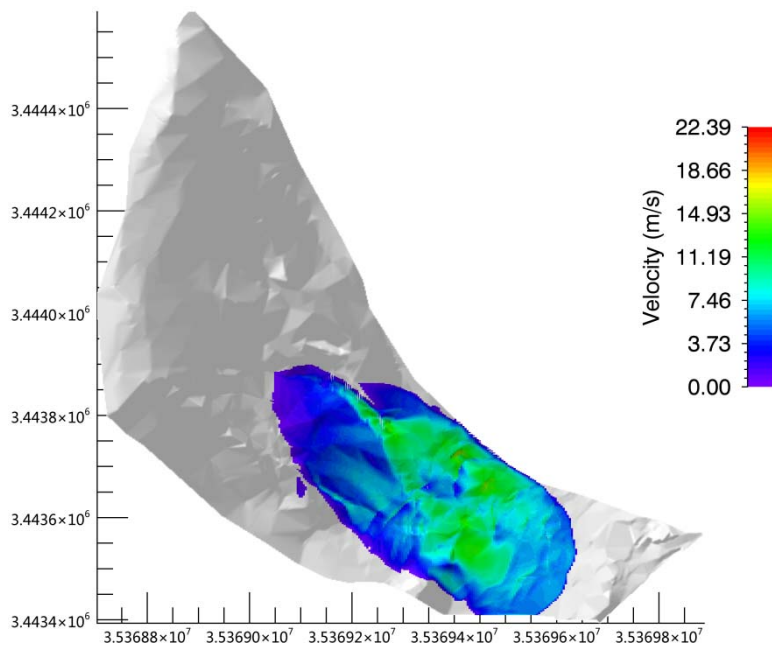
Unit weight $\gamma(kN \cdot m^{-3})$	Coulomb friction coefficient μ	Viscous friction coefficient $\zeta(m \cdot s^{-2})$	Erosional entrainment rate k_i
20.8	0.45	500	0.0001



284

(a) Flow height

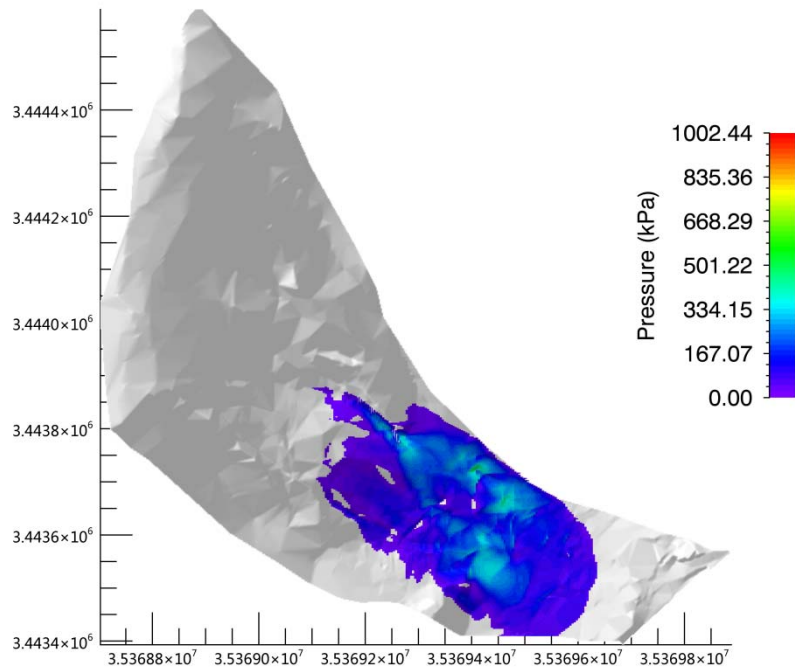
285



286

(b) Velocity

287



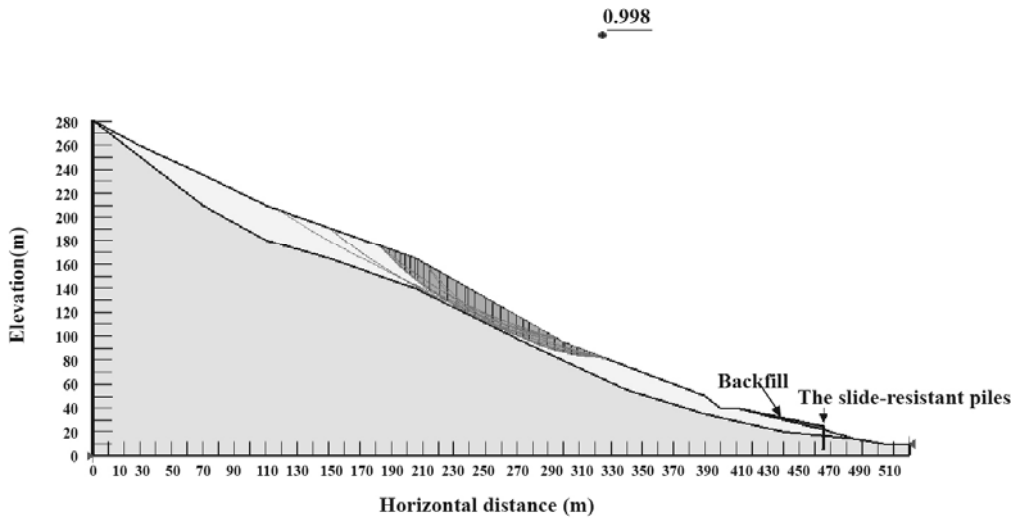
(c) Pressure

Fig. 7 Movement characteristic parameters of the Taziping landslide (before treatment)

See the kinematic characteristic parameters of the landslide deposits in Fig.7. The colored bar shows the maximum values of the kinematic process for a given time step. As shown by the calculation results, deposits accumulated during the landslide movement process had a maximum flow height of 23.85m, located around the surface gully of the middle and upper slope. The middle and lower section of the landslide deposit had a flow height of about 5-10m; the middle and lower movement velocity of the landslide ranged from 3m/s and 7m/s; the landslide had a mean pressure of about 500kPa, and the pressure of the middle and lower deposits was about 200kPa. Thus, three-story and lower houses within the deposition range might be buried (The building is 3m high on each floor), and it was further suggested that the design strength of the gable walls of houses on the middle and upper parts of the deposit be increased above 300kPa.

3.3 Hazard prediction after treatment

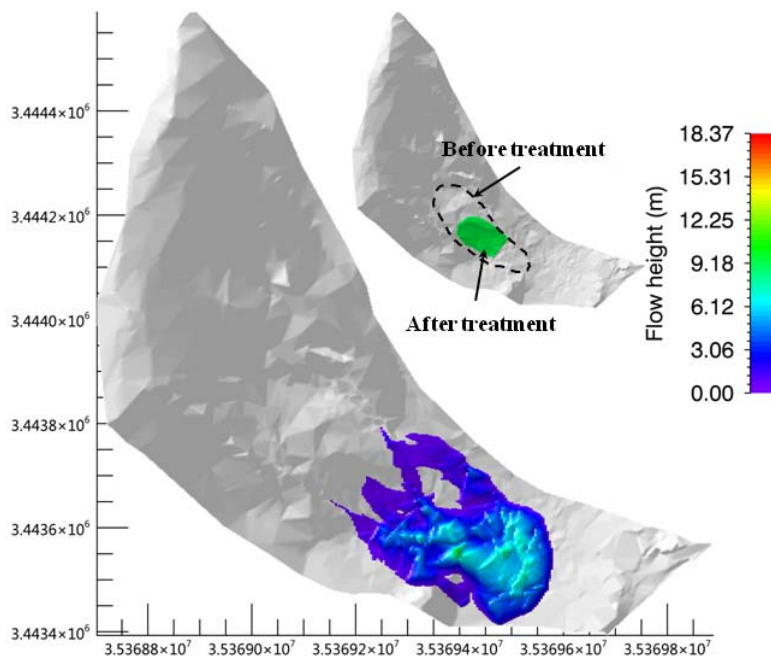
After fully accounting for the slide-resistant piles and mounds, we introduced the Morgenstern-Price method (Morgenstern et al., 1965) to calculate the stability coefficient of Taziping landslide after treatment. The method was determined with an iterative approach by changing the position of the sliding surface until failure of the dumpsite (Fig.8). The physico-mechanical parameters under a saturated state (Hydrologic Engineering and Geological Survey Institute of Hebei Province, 2010) were adopted to search for the sliding plane of the landslide.



313

314 Fig.8 Search for the sliding plane of the Taziping landslide (before treatment)

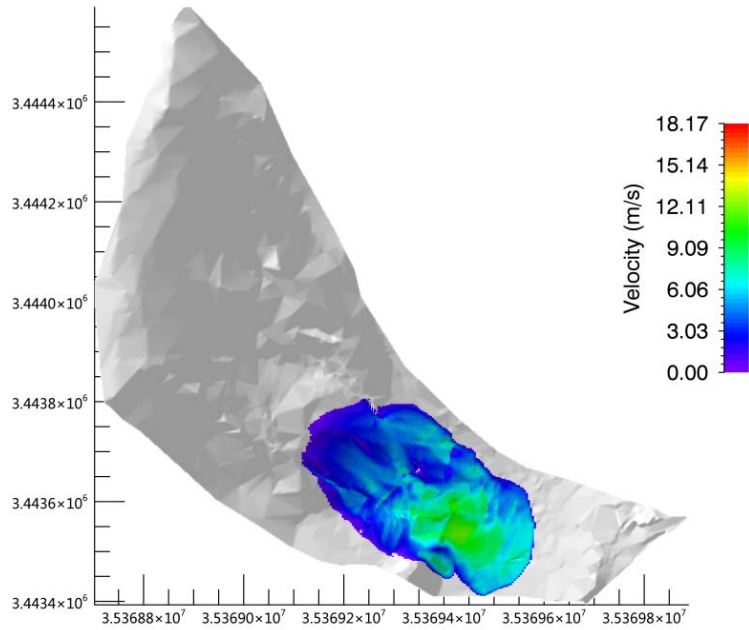
315 Based on numerical analysis, the Taziping landslide stability coefficient is 0.998.
 316 Under rainfall conditions, the middle area of the Taziping landslide was unstable.
 317 Loose deposits in the middle part of the landslide might convert into a high-water
 318 landslide and cut out from the top of the slide-resistant piles. In the damaged area, the
 319 slope had a rear edge wall elevation of about 1,170m. Its front edge was located on
 320 the south side of the mountain road, with an elevation of 1,070-1,072m and a length
 321 of 182m. Thus, the scale of the rainfall-damaged is estimated to be about 250,000m³,
 322 with a mean thickness of about 6m. The parameters in Tab.2 were again adopted for
 323 the simulated calculation.



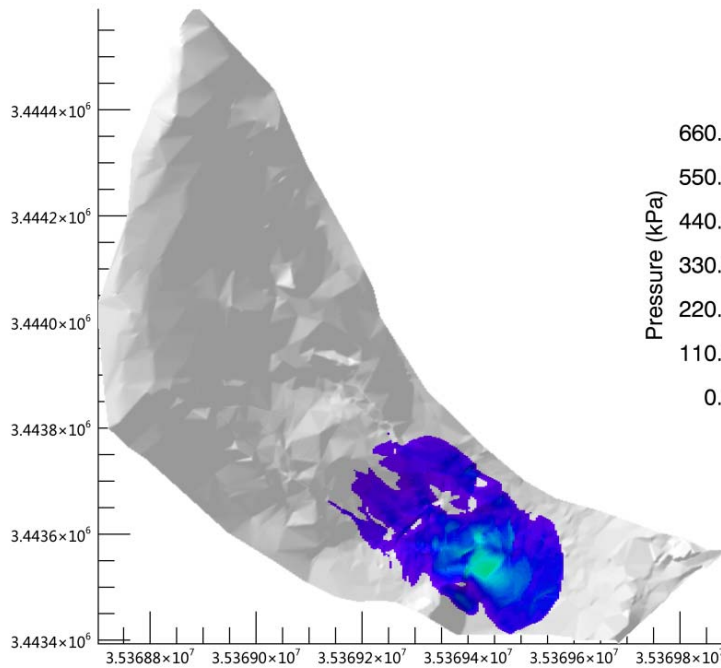
324

325

(a) Flow height



(b) Velocity



(c) Pressure

326
327

328
329

330 Fig. 9 Movement characteristic parameters of the Taziping landslide (after treatment)

331 Provided in Fig.9 are the kinematic characteristics of the landslide deposit. The
 332 colored bar shows the maximum values of the kinematic process for a given time step.
 333 Deposits accumulated during the landslide movement process had a maximum flow height of 18.37m, located around the surface gully of the middle and upper slope. The
 334 middle and lower portions of the landslide deposit had a flow height of approximately
 335 3-5m. The middle and lower movement velocity of the landslide deposits ranged
 336 3-5m.

337 between 3m/s and 5m/s. The landslide had a mean pressure of about 330kPa, and the
 338 pressure of the middle and lower deposits was about 100kPa. Thus, it could be held
 339 that two-story and lower houses within the deposition range might be buried. It was
 340 further suggested that the design strength of the gable walls of houses on the middle
 341 and upper parts of the deposits be increased above 150kPa.

342 After treatment, the accumulation flow height and pressure of the deposits were
 343 reduced by about 1/2, and the kinematic speed is reduced by about 1/3. However, the
 344 Miaoba residential area of Red Village was still partially at hazard.

345

346 4 Results

347 Landslides reflect landscape instability that evolves over meteorological and
 348 geological timescales, and they also pose threats to people, property, and the
 349 environment. The severity of these threats depends largely on landslide speed and
 350 travel distance. There may be examples where entire houses on a landslide mass are
 351 moved but not destroyed because of stable base plates. In any case, velocity plays a
 352 more important role regarding kinetic energy acting on an obstacle. However, the
 353 Miaoba residential area of Red Village is located at the frontal part of Tazhiping
 354 landslide. During landslide movement, the spatial scale indexes of a landslide mass
 355 include area, volume, and thickness. The maximum thickness of the landslide is one
 356 of the direct factors influencing the building's deformation failure status. A large
 357 landslide displacement may lead to burial, collapse, or deformation failure of the
 358 building, and thus influence its safety and stability. Thus, landslide thickness
 359 constitutes an important index for assessing the hazards of a landslide disaster, and for
 360 influencing the consequences faced by disaster-affected bodies (Fell et al., 2008;
 361 DZ/T, 0286-2015). Provided in Tab.3 is a landslide thickness-based division of the
 362 predicted hazard zones of Taziping landslide, in which the thickness of the landslide
 363 mass correlates with the ability of a building to withstand a landslide disaster (Hung
 364 et al., 1984; Petrazzuoli et al., 2004; Glade 2006; GB, 50010–2010; Hu et al., 2012;
 365 Zeng et al., 2015). After treatment with slide-resistant piles, the hazard of a future
 366 slide was reduced by about 1/3 overall and by 2/3 in high-hazard zones.

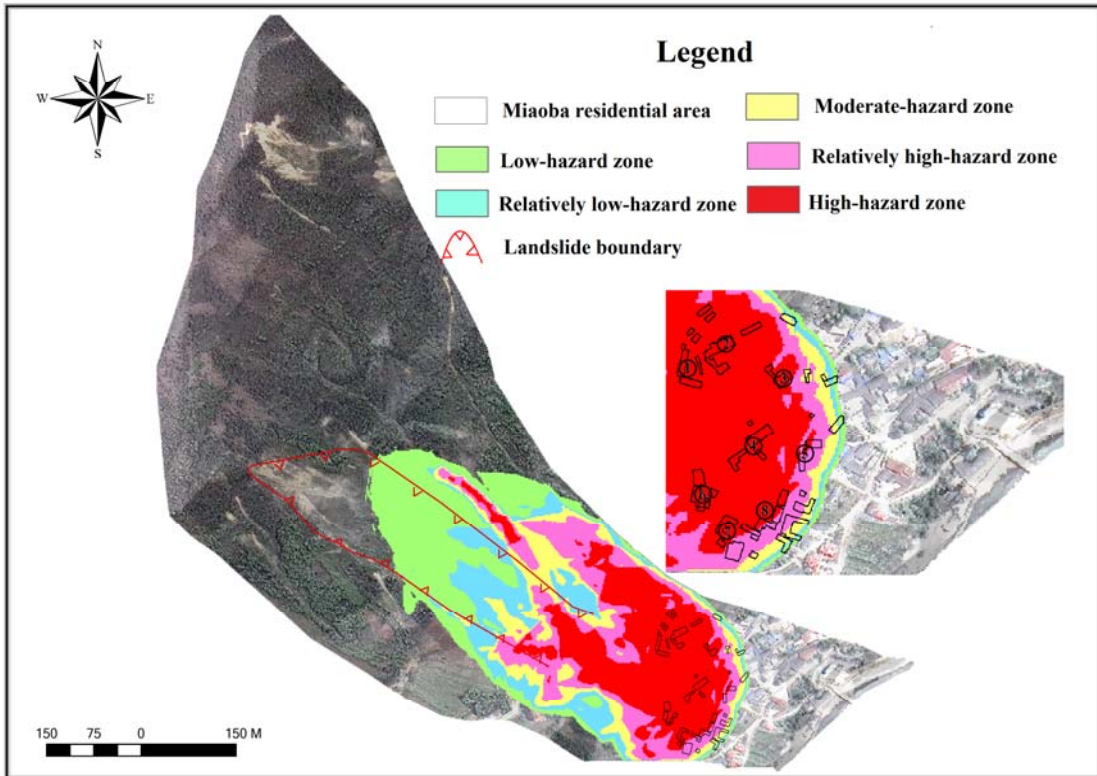
367 **Tab.3 Division table of the predicted hazards of Taziping landslide (unit: m²)**

Hazard zone level	Assessment index	Building damage probability	Area before treatment	Area after treatment	Increased/decreased area	Building damage characteristics
Low-hazard zone (I)	$h \leq 0.5\text{m}$	20%	44 , 600	38 , 748	-5,852	One-story houses may be damaged; houses on the

						landslide mass are partially damaged.
						One-story houses have a very high probability of being damaged; one-story houses on the landslide mass are completely damaged.
Relatively low-hazard zone (II)	$0.5\text{ m} < h \leq 1\text{ m}$	50~20%	24 , 900	26 , 400	+1,500	One-story to three-story houses have a very high probability of being damaged; houses less than three stories on the landslide mass are completely damaged.
Moderate-hazard zone (III)	$1\text{ m} < h \leq 3\text{ m}$	80~50%	21 , 980	15 , 856	-6,124	One-story houses may be buried, and two-story to six-story houses have a very high probability of being damaged; houses on the landslide mass are completely
Relatively high-hazard zone (IV)	$3\text{ m} < h \leq 5\text{ m}$	100~80%	30 , 820	19 , 636	-11,184	are completely

						damaged.
						Two-story and
						lower houses may
						be buried, and
						three-story and
High-hazard						higher houses have
zone	$h \geq 5\text{m}$	100%	47 , 240	13 , 052	-34,188	a very high
(V)						probability of being
						damaged; houses on
						the landslide mass
						are completely
						damaged.
Total area:	—	—	169 , 540	113 , 700	-54,340	—

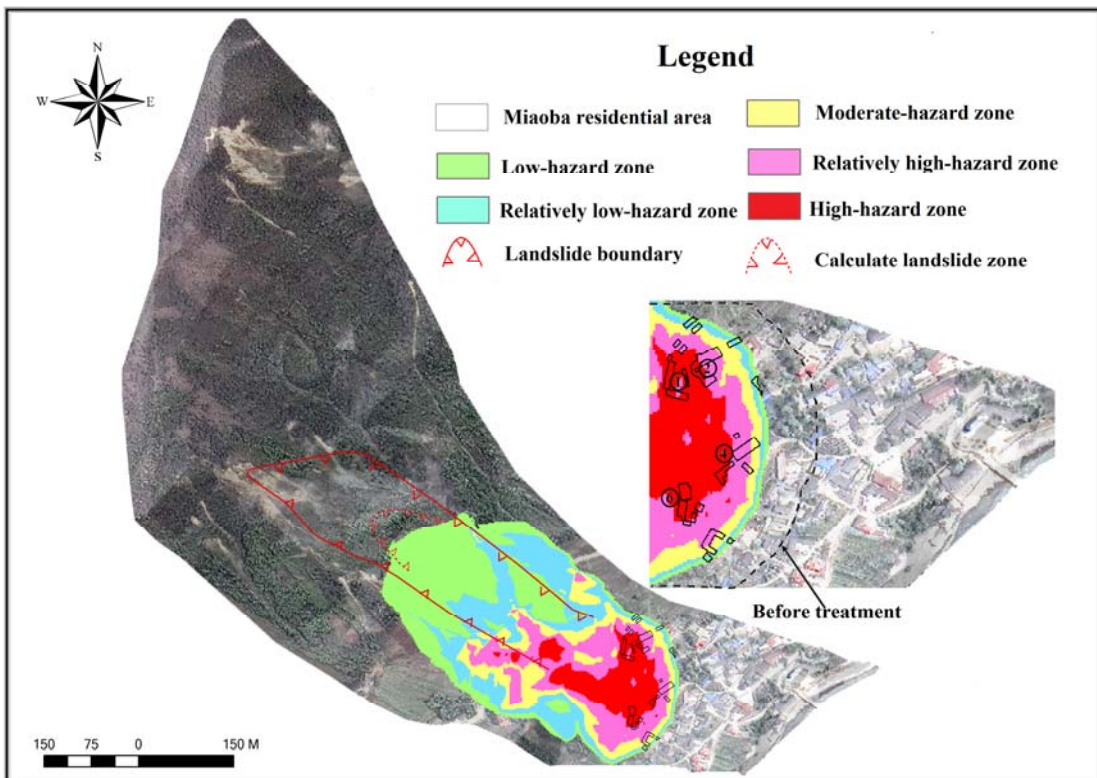
368 The hazard zones of Taziping landslide was given by 2D divisions before and
369 after engineering treatment (Fig. 10). The size of the hazard zones changed after
370 engineering treatment, particularly in the high-hazard zones. Before treatment with
371 slide-resistant piles, the landslide posed a great hazard to eight houses on the left side
372 of the upper Miaoba residential area, with a high-hazard zone associated with
373 landslide mass height over 5m and a red zone. After treatment, the number of effected
374 houses was reduced to four. We defined outside the colored area as no-hazard.



375

376

(a) Before treatment



377

378

379

380

(b) After treatment

Fig. 10 2D division comparison of the hazards of the Taziping landslide

381 5 Conclusions and Discussion

382 The hazard assessment of landslides using numerical models is becoming more
383 and more popular as new models are developed and become available for both
384 scientific research and practical applications. There is some confusion about the mass
385 movement process that is discussed by the rheological model presented in this
386 contribution.

387 Landslides move downslope in many different ways (Varnes, 1978). In addition,
388 landslides can evolve into rapidly travelling flows, which exhibit characteristics of
389 debris flows on unchannelized or only weakly channelized hillslopes. The
390 geomorphic heterogeneity of rapid shallow landslides, such as hillslope debris flows,
391 is larger than observed in channelized debris flows; however many of these flows can
392 be successfully modelled using the Voellmy-fluid friction (Christen et al., 2012).
393 Results presented in this paper support the conclusion that Voellmy-fluid rheological
394 model can be used to simulate flow-type landslides.

395 The selection of model parameters remains one of the fundamental challenges
396 for numerical calculations of natural hazards. At present, there are numerous
397 empirical parameters obtained from 30-years of monitoring data. Such as in RAMMS,
398 we can automatically generate the friction coefficient of an avalanche for our
399 calculation domain based on topographic data analysis, forest information and global
400 parameters (WSL, 2013). The friction parameters for debris flows can found in some
401 literature (Fannin et al., 2001; Iovine et al., 2003; Hürlimann et al., 2008; Scheidl et
402 al., 2010; Huang et al., 2015). However, there is little research regarding friction
403 parameters of flow-type landslide. Therefore, we tested different coulomb friction
404 coefficient μ values ranging between $0.1 \leq \mu \leq 0.6$ and viscous friction coefficient ζ
405 values ranging between $100 \leq \mu \leq 1000 m \cdot s^{-2}$. Finally, we selected the coulomb
406 friction coefficient $\mu = 0.45$ and viscous friction coefficient $\zeta = 500 m \cdot s^{-2}$ in
407 accordance with back-analyses of well-documented landslides (Cepeda et al., 2010;
408 Du et al., 2015). Simulation results are consistent with field observations of
409 topography and sliding path.

410 Based on the finite volume method and the RAMMS program, simulation results
411 of Taziping landslide were consistent with the sliding path predicted by the field
412 investigation. This correlation indicates that numerical simulation is an effective
413 method for studying the movement processes of flow-type landslides. The
414 accumulation flow height and pressure of landslide deposits were reduced by about
415 1/2, and the kinematic speed was reduced by about 1/3 after treatment. However, the
416 Miaoba residential area of Red Village is still partially at hazard. Considering that
417 two-story and lower houses within the deposition range might be buried, it was further
418 suggested that the design strength of the gable walls of houses on the middle and
419 upper parts of the deposit be increased above 150kPa.

420 By utilizing a GIS platform in combination with landslide hazard assessment
421 indexes, we mapped the 2D division of the Taziping landslide hazard zones before

422 and after engineering treatment. The results indicated that overall hazard zones
423 contracted after engineering treatment and, the area of high-hazard zones was reduced
424 by about 2/3. After engineering treatment, the number of at hazard houses on the left
425 side of the upper Miaoba residential area, was reduced from eight to four. It was thus
426 clear that some zones are still at high hazard despite engineering treatment. Therefore,
427 it was proposed that houses located in high-hazard zones be relocated or reinforced
428 for protection.

429

430

431

432 **Acknowledgments**

433 The authors sincerely acknowledge the CAS Pioneer Hundred 432 Talents
434 Program for the completion of this research. This work was supported by National
435 Natural Science Foundation of China (Grant No. 41301009 41301592) and the
436 Hundred Young Talents Program of IMHE (SDSQB-2016-01), the International
437 Cooperation Program of the Ministry of Science and Technology of China (Grant
438 No.2013DFA21720). The authors express their deepest gratitude to those aids and
439 assistances. The authors also extend their gratitude to editor and two anonymous
440 reviewers for their helpful suggestions and insightful comments, which have
441 contributed greatly in improving the quality of the manuscript.

442

443

444

445 **Reference**

- 446 Bartelt, P., Bühler, Y., Buser, O., Christen, M., and Meier, L.: Modeling massdependent flow
447 regime transitions to predict the stopping and depositional behavior of snow avalanches, *J.*
448 *Geophys. Res.*, 117, F01015, doi:10.1029/2010JF001957, 2012 .
- 449 Costa, J.E.: Physical geomorphology of debris flows. *Developments and Applications of*
450 *Geomorphology*, Springer Press., 268-317, 1984.
- 451 Christen, M., Kowalski, J., and Bartelt, P.: RAMMS: Numerical simulation of dense snow
452 avalanches in three-dimensional terrain, *Cold Regions Science and Technology.*, 63, 1–14,
453 2010.
- 454 Christen, M., Bartelt, P., and Kowalski, J.: Back calculation of the In den Arelen avalanche with
455 RAMMS: interpretation of model results, *Annals of Glaciology.*, 51, 161–168, 2010.
- 456 Christen, M., Bühler, Y., Bartelt, P., Leine, R., Glover, J., Schweizer, A., Graf, C., McArdeLL, B.,
457 Gerber, W., Deubelbeiss, Y., Feistl, T., and Volkwein, A.: Integral hazard management using a
458 unified software environment: numerical simulation tool “RAMMS” for gravitational natural
459 hazards, In: Koboltschnig, G., Hübl, J., Braun, J. (eds.) *Proceedings of 12th Congress*
460 *INTERPRAE.*, 1, 77–86, 2012.
- 461 Chen, J.C., and Chuang, M.R.: Discharge of landslide-induced debris flows: case studies of
462 Typhoon Morakot in southern Taiwan, *Nat. Hazards Earth Syst. Sci.*, 14, 1719-1730, 2014.
- 463 Cepeda, J., Chávez, J.A., and Martínez, C.C.: Procedure for the selection of runout model
464 parameters from landslide back-analyses: application to the Metropolitan Area of San

465 Salvador, El Salvador, *Landslides.*, 7, 105–116, 2010.

466 Du, J., Yin, K.L., and Wang, J.J.: Simulation of three-dimensional movement of landslide-debris
467 flow based on finite volume method, *Chinese Journal of Rock Mechanics and Engineering.*,
468 34: 480–488, 2015 (in Chinese).

469 Evans, S.G., Tutubalina, O.V., Drobyshev, V.N., Chernomorets, S.S., McDougall, S., Petrakov,
470 D.A., and Hungr, O.: Catastrophic detachment and high-velocity long-runout flow of Kolka
471 Glacier, Caucasus Mountains, Russia in 2002, *Geomorphology.*, 105, 314–321, 2009.

472 Fannin, R.J., and Wise, M.P.: An empirical-statistical model for debris flow travel distance,
473 *Canadian Geotechnical Journal.*, 38, 982–994, 2001.

474 Finlay, P.J., Mostyn, G.R., and Fell, R.: Landslide risk assessment: prediction of travel distance,
475 *Canadian Geotechnical Journal.*, 36, 556–562, 1999.

476 Fell, R., Corominas, J., Bonnard, C., Cascini, L., Leroi, E., and Savage, W. Z.: Guidelines for
477 landslide susceptibility, hazard and risk zoning for land use planning, *Engineering Geology.*,
478 102, 85–98, 2008.

479 Fannin, R., and Wise, M.: An empirical-statistical model for debris flow travel distance, *Can*
480 *Geotech J.*, 38, 982–994, 2001.

481 Glade, T.: Linking debris-flow hazard assessments with geomorphology. *Geomorphology.*, 66(1):
482 189-213, 2005.

483 Glade, T., Anderson, M. G., Crozier, M.J.: *Landslide hazard and risk.* Wiley., 75-138, 2006.

484 GB 50010–2010.: Code for design concrete structures, Beijing: Chinese Architectural Industry.,
485 34–80, 2010 (in Chinese).

486 Hebei Province Institute of Hydrogeological and Engineering.: Geological investigation
487 engineering supplemental survey report of Hongse Village Taziping landslide in Hongkou
488 Town of Dujiangyan City, Sichuan Province., 2010 (in Chinese).

489 Hungr, O.: A Model for the runout analysis of rapid flow slides, debris flows and avalanches, *Can*
490 *Geotech J.*, 32, 610–623, 1995.

491 Hungr, O., Evans, S.G, Bovis, M.J., and Hutchinson, J.N.: A review of the classification of
492 landslides of the flow type, *Environ Eng Geosci.*, 7, 221–238, 2001.

493 Hungr, O., Morgan G.C., and Kellerhals, R.: Quantitative analysis of debris torrent hazards for
494 design of remedial measures, *Can Geotech J.*, 21, 663–677, 1984.

495 Hu, K.H., Cui, P., and Zhang, J.Q., Characteristics of damage to buildings by debris flows on 7
496 August 2010 in Zhouqu, Western China, *Nat Hazards Earth Syst Sci.*, 12, 2209–2217, 2012.

497 Hürlimann, M., Rickenmann, D., Medina, V., and Bateman, A.: Evaluation of approaches to
498 calculate debris-flow parameters for hazard assessment, *Eng Geol.*, 102, 152–163, 2008.

499 Huang, Y., Cheng, H., Dai, Z., Xu, Q., Liu, F., Sawada, K., Moriguchi, S., and Yashima, A.:
500 SPH-based numerical simulation of catastrophic debris flows after the 2008 Wenchuan
501 earthquake, *Bull Eng Geol Environ.*, 74, 1137–1151, 2015.

502 Iverson, R. M., Reid, M. E., and LaHusen, R. G.: Debris-flow mobilization from landslides, *Annu.*
503 *Rev. Earth Planet Sc.*, 25, 85– 138, 1997.

504 Iverson, R.M., and Vallance, J.W.: New views of granular mass flows, *Geology.*, 29, 1115–1118,
505 2001.

506 Iovine, G., Gregorio, S.D., and Lupiano, V.: Debris-flow susceptibility assessment through cellular
507 automata modeling: an example from 15–16 December 1999 disaster at Cervinara and San
508 Martino Valle Caudina (Campania, southern Italy), *Nat Hazards Earth Syst Sci.*, 3, 457–468,

509 2003.

510 Jackson, L.E., Kostashuk, R.A., and MacDonald, G.M.: Identification of debris flow hazard on
511 alluvial fans in the Canadian Rocky mountains, *Geological Society of America.*, 7, 155–124,
512 1987.

513 LeVeque, R.: *Finite Volume Methods for Hyperbolic Problems*, Cambridge Texts in Applied
514 Mathematics Cambridge University Press., 2002.

515 Michael-Leiba, M., Baynes, F., Scott, G., and Granger, K.: Regional landslide risk to the Cairns
516 community, *NatHazards.*, 30, 233–249, 2003.

517 Morgenstern, N.R., and Price, V.E.: The analysis of the stability of general slip surfaces,
518 *Geotechnique.*, 15, 79–93, 1965.

519 Portilla, M., Chevalier, G., and Hürlimann, M.: Description and analysis of the debris flows
520 occurred during 2008 in the Eastern Pyrenees, *Nat. Hazards Earth Syst. Sci.*, 10, 1635–1645,
521 2010.

522 Petrazzuoli, S.M., and Zuccaro, G.: Structural resistance of reinforced concrete buildings under
523 pyroclastic flows: a study of the Vesuvian area, *J Volcanol Geoth Res.*, 133, 353–367, 2004.

524 Sassa, K., Nagai, S., Solidum, R., Yamazaki, Y., and Ohta, H.: An integrated model simulating the
525 initiation and motion of earthquake and rain induced rapid landslides and its application to
526 the 2006 Leyte landslide, *Landslides.*, 7, 219–236, 2010.

527 Scott, K.M., and Vallance, J.W.: *History of Landslides and Debris Flows at Mount Rainier: Water
528 Fact Sheet*, USGS Open-File Report., 93–111, 1993.

529 Shi, G.H.: *Discontinuous deformation analysis - a new numerical model for the statics and
530 dynamics of block system*, Berkeley: University of California., 1988.

531 DZ/T 0286-2015.: *Specification of risk assessment for geological hazard*, Ministry of Land and
532 Resources of the People's Republic of China., 2015 (in Chinese).

533 Scheidl, C., and Rickenmann, D.: Empirical prediction of debris-flow mobility and deposition on
534 fans, *Earth Surf Proc Land.*, 35, 157–173, 2010.

535 Toro, E.F.: Riemann problems and the waf method for solving the two dimensional shallow water
536 equations. *Philos. Trans. R. Soc. London., Ser. A* 338, 43–68, 1992.

537 Varnes, D.J., : Slope movement types and processes. In: Schuster RL, Krizek RJ (eds) *Landslides:
538 analysis and control*. Transportation Research Board, National Research Council, Washington,
539 DC, USA., 11–33 , 1978.

540 Wang, L., Li, B., Gao, Y., and Zhu, S.: Run-out prediction of large thick-bedded unstable rock: A
541 case study of Daxiang unstable rock in Yangjiao town, Wulong county, Chongqing, *Earth
542 Science Frontiers.*, 23, 251–259, 2016 (in Chinese).

543 WSL.: *RAMMS: A numerical model for snow avalanches in research and practice*, User manual
544 v1.5 avalanche, WSL Institute for snow and avalanche research SLF, Swiss., 2013.

545 Zeng, C., Cui, P., Su, Z.M., Lei, Y., Chen, R.: Failure modes of reinforced concrete columns of
546 buildings under debris flow impact, *Landslides.*, 12, 561-571, 2015.